ARMY RESEARCH LABORATORY

Outer Scale and Diffraction Influences on Observed Angle-of-Arrival Variance

by David H. Tofsted

ARL-TR-6231 October 2012

NOTICES

Disclaimers

The findings in this report are not to be construed as an official Department of the Army position unless so designated by other authorized documents.

Citation of manufacturer's or trade names does not constitute an official endorsement or approval of the use thereof.

Destroy this report when it is no longer needed. Do not return it to the originator.

Army Research Laboratory

White Sands Missile Range, NM 88002-5501

ARL-TR-6231 **October 2012**

Outer Scale and Diffraction Influences on Observed Angle-of-Arrival Variance

David H. Tofsted

Computational and Information Sciences Directorate, ARL

REPORT DOCUMENTATION PAGE	Form Approved OMB No. 0704-0188

1. REPORT DATE *(DD-MM-YYYY)*	2. REPORT TYPE	3. DATES COVERED (From - To)
October 2012	Final	05 2012–08 2012

4. TITLE AND SUBTITLE
Outer Scale and Diffraction Influences on Observed Angle-of-Arrival Variance

5a. CONTRACT NUMBER

5b. GRANT NUMBER

5c. PROGRAM ELEMENT NUMBER

6. AUTHOR(S)
David H. Tofsted

5d. PROJECT NUMBER

5e. TASK NUMBER

5f. WORK UNIT NUMBER

7. PERFORMING ORGANIZATION NAME(S) AND ADDRESS(ES)
U.S. Army Research Laboratory
ATTN: RDRL-CIE-D
White Sands Missile Range, NM 88002-5501

8. PERFORMING ORGANIZATION REPORT NUMBER
ARL-TR-6231

9. SPONSORING/MONITORING AGENCY NAME(S) AND ADDRESS(ES)

10. SPONSOR/MONITOR'S ACRONYM(S)

11. SPONSOR/MONITOR'S REPORT NUMBER(S)

12. DISTRIBUTION/AVAILABILITY STATEMENT
Approved for public release; distribution is unlimited.

13. SUPPLEMENTARY NOTES
primary author's email: <david.h.tofsted.civ@mail.mil>

14. ABSTRACT

Analysis of turbulence distorted imagery may allow turbulence strength (C_n^2) to be estimated based on observed object motions (angle-of-arrival variations) in multi-frame image sequences. Such estimation methods would be useful when measured scintillometer data is unavailable, but should account for outer scale and diffraction effects, as these may influence the C_n^2 turbulence strength prediction. The present paper analyzes these effects on single-axis angle-of-arrival variance for the case of spherical wave propagation and homogeneous turbulence properties. The analysis indicates outer scale influences may be significant, depending on the height of the line of sight and the system aperture size.

15. SUBJECT TERMS
Turbulence, angle of arrival, outer scale, diffraction

16. SECURITY CLASSIFICATION OF:			17. LIMITATION OF ABSTRACT	18. NUMBER OF PAGES	19a. NAME OF RESPONSIBLE PERSON
a. REPORT	b. ABSTRACT	c. THIS PAGE			David H. Tofsted
Unclassified	Unclassified	Unclassified	UU	26	19b. TELEPHONE NUMBER (*Include area code*) 575-678-3039

Contents

List of Figures

1. Introduction

In a recent paper a new method was described to evaluate the short–exposure Modulation Transfer Function (MTF) (Tofsted, 2011). Part of that reanalysis evaluated diffraction-related effects on the phase structure function which impacted both the angle-of-arrival variance and a phase-tilt correlation term. However, that analysis considered only Kolmogorov turbulence (no outer scale of turbulence influence). The outer scale is well known to affect angle-of-arrival (e.g., Tofsted, 1992), but that and other analyses did not consider aperture effects leading to diffraction influences. To study the outer scale influence, the low frequency portion of the refractive index spectrum must first be modeled, then its impacts on the angle-of-arrival must be evaluated numerically. This low frequency influence is parameterized relative to the outer scale of turbulence, L_o.

For completeness, we begin by considering prior angle-of-arrival variance formulations, as reported by Beland (1993) and Dror and Kopeika (1995). Beland (1993) provided a formula for plane wave angle-of-arrival variance:

$$\langle \alpha^2 \rangle = 2.91\, D^{-1/3} \int_0^L C_n^2(z)\, \mathrm{d}z, \tag{1}$$

where D is the system entrance pupil diameter [m], L is the path length [m], z is the path variable, and C_n^2 is the refractive index structure parameter [$\mathrm{m}^{-2/3}$].

Dror and Kopeika (1995) suggested the spherical wave single-axis angle-of-arrival variance formula,

$$\langle \alpha_x^2 \rangle = 2.92\, D^{-1/3} \int_0^L C_n^2(z) \left(\frac{z}{L}\right)^{5/3} \mathrm{d}z, \quad Z < 1 \ll Q, \tag{2}$$

where diffraction and outer scale related dimensionless scales are introduced: $Q = D/(\lambda\, L)^{1/2}$ and $Z = D/L_o$, where λ is the propagation wavelength. (Note, Dror and Kopeika claimed equation 2 was a single-axis result, but comparison with equation 1 indicates a discrepancy. Either the Dror and Kopeika result is too large by a factor of two, or the Beland result is too small by a factor of two.)

The current study extends the above results to include outer scale and diffraction effects (dependence on Q and Z variables) for the spherical wave case. For tabulation purposes the diffraction and outer scale effects are studied under conditions of homogeneous turbulence.

Motivating this study is the application where measured angle-of-arrival variance is used to predict turbulence strength, C_n^2. That is, experiments specifically designed to study the impacts of turbulence typically measure turbulence strength directly using one or more scintillometers. In other circumstances collected imagery may exhibit turbulence impacts but lack corresponding turbulence measurements. Further, some imaging configurations may preclude the use of scintillometers, for example if objects of interest are airborne. Hence, if imagery alone can be analyzed to estimate C_n^2, this extends the potential analysis of turbulence effects to greater numbers of data sets.

For this case, it is important to know how outer scale and diffraction effects are impacting the estimates of turbulence via angle-of-arrival. As will be shown, while the error is not great, including outer scale effects adds an additional source of error to the calculations. The remainder of the paper is devoted to resolving how to evaluate the angle-of-arrival variance given knowledge of the turbulence strength, outer scale, and optical problem geometry. We first overview the calculation in section 2, but leave the final resolution of the analysis to section 4. Between these two, in section 3 we introduce the revised von-Kármán (RvK) spectrum first described in Tofsted et al. (2007), including the definition for the outer scale given in terms of height above the ground and the Obukhov length (e.g., Obukhov, 1946; Paulson, 1970).

2. General Angle-of-Arrival Variance Calculation Procedure

In this section we overview the angle-of-arrival variance calculation procedure. Let $\langle \alpha^2 \rangle$ be the angle-of-arrival variance, assumed isotropic such that x and y axis components are equal. To model this variance, the basic tilt calculation included in Fried's (1966) short-exposure imaging paper is adapted. That approach considered the phase produced by a point source and propagated a distance L to the entrance pupil of a circular aperture system. There, Fried's main integral form was integrated in the aperture. Fried considered the propagated phase could be expressed as a function $\phi(\boldsymbol{v})$, of the two-dimensional vector in the transverse plane of the receiver entrance pupil, $\boldsymbol{v}$.

Fried considered that the tilt effect could be parameterized by a vector, $\boldsymbol{a}$, whose dimensions are that of inverse length (m^{-1}), to represent the mean tilt of the incident phase across the aperture. This vector permits a new tilt-corrected phase function to be defined, as $\psi(\boldsymbol{v}) = \phi(\boldsymbol{v}) - \boldsymbol{a} \cdot \boldsymbol{v}$, in the system entrance pupil.

The variance of $\boldsymbol{a}$ could be expressed in integral form in the system aperture by,

$$\langle \boldsymbol{a} \cdot \boldsymbol{a} \rangle = \frac{64}{D^2} \int_0^1 u \, \mathrm{d}u \, \left[\mathcal{F}_C(u) - \mathcal{F}_L(u) \right] \mathcal{D}_\phi(Du), \tag{3}$$

where functions $\mathcal{F}_C(u)$ and $\mathcal{F}_L(u)$ are given by,

$$\begin{aligned} \mathcal{F}_C(u) &= (2/\pi) \left(\cos^{-1}(\omega) - \omega \sqrt{1-\omega^2} \right), \\ \mathcal{F}_L(u) &= (2/\pi) \left(3 \cos^{-1}(\omega) - \omega \left[7 - 4\,u^2 \right] \sqrt{1-\omega^2} \right), \end{aligned} \tag{4}$$

and where $\mathcal{D}_\phi(\rho)$ is the phase structure function (e.g., Goodman, 1985) for a transverse separation distance ρ in the system aperture.

The vector $\boldsymbol{a}$ physically represents the rate of phase change per unit distance in the system aperture. This vector is transformed into an angular dimension by dividing the variance of $\boldsymbol{a}$ by the wavenumber ($k = 2\pi/\lambda$). The $\boldsymbol{a}$ variance can thus be transformed into an angular variance via:

$$\langle \boldsymbol{\alpha} \cdot \boldsymbol{\alpha} \rangle = \langle \boldsymbol{a} \cdot \boldsymbol{a} \rangle / k^2. \tag{5}$$

This transformation is based on an argument using similar triangles.

The key to extending these results beyond Kolmogorov turbulence is to include outer scale influences in the phase structure function calculation. For spherical wave propagation this function is given as,

$$\mathcal{D}_\phi(\rho) = 8\,\pi^2\,k^2\,L \int_0^1 \mathrm{d}c \int_0^\infty \kappa \, \mathrm{d}\kappa \, \Phi_n(\kappa) \, \left[1 - J_0(\kappa\, c\, \rho) \right] \, \cos^2 \left[\frac{\kappa^2 \, \lambda \, L \, c(1-c)}{4\pi} \right]. \tag{6}$$

where c is a normalized path variable ($c = z/L$), κ [m^{-1}] is the spatial frequency in which the turbulence spectrum $\Phi_n(\kappa)$ is expressed, and $J_0(x)$ is the Bessel function of the first kind order zero.

Notice that in equation 3 $\mathcal{D}_\phi$ utilizes the normalized distance argument $u = \rho/D$. In Tofsted (2011), it was shown that when invoking constant Kolmogorov turbulence the phase structure function could be expressed as a product of the wave structure function, $\mathcal{D}(\rho)$, with a function, denoted $\alpha(R)$, accounting for the diffraction influence arising from the argument of the cosine-squared term in the phase structure function's inner integral. Comparison with the wave structure function's integral definition is useful:

$$\mathcal{D}(\rho) = 8\,\pi^2\,k^2\,L \int_0^1 \mathrm{d}c \int_0^\infty \kappa \, \mathrm{d}\kappa \, \Phi_n(\kappa) \, \left[1 - J_0(\kappa\, c\, \rho) \right]. \tag{7}$$

The phase structure function's integral form approaches that of the wave structure function whenever the argument of the cosine-squared term remains small throughout integration. The argument of $\alpha(R)$ is the normalized length scale $R = \rho/P$ where $P = \sqrt{\lambda L}$, the Fresnel zone, such that $R = u\,D/P = u\,Q$.

This construction, $\mathcal{D}_\phi(uD) = \mathcal{D}(uD)\,\alpha(uQ)$, is possible because the Kolmogorov refractive index spectrum,

$$\Phi_n(\kappa) = \Phi_K(\kappa) = \beta\,C_n^2\,\kappa^{-11/3}, \tag{8}$$

contains only the single parameter, C_n^2, and where β is an integration constant,

$$\beta = (5/36)\,\left[2^{2/3}\,\Gamma(5/6)\right] / \left[\pi^{3/2}\,\Gamma(2/3)\right] \approx 0.033. \tag{9}$$

connecting the Kolmogorov spectrum to the unrestricted refractive index structure function,

$$\mathcal{D}_n(r) = \mathcal{D}_K(r) = C_n^2\,r^{2/3}. \tag{10}$$

In the case of homogeneous turbulence, C_n^2 factors out of both structure function integrals. In the case of the phase structure function, the remaining double integral becomes a function of only R.

This simplified result is considerably complicated by the introduction of an outer-scale dependence in the refractive index spectrum, as discussed in the following section.

3. Revised von Kármán Spectrum

The influence of the outer scale of turbulence on angle-of-arrival measurements is to introduce a low frequency cutoff in the spectrum. The form used to model the outer scale effect was first introduced in 2007 (Tofsted, 2007). The revised von-Kármán (RvK) spectrum is based on von-Kármán's (1948) recommendation that the low frequency dependence in the spectrum should exhibit κ^2 behavior. In this section we describe this spectrum and define the outer scale behavior in the atmospheric surface layer. In particular, we define the outer scale as a function of height above the surface (optical line-of-sight height) as well as the Obukhov length $\mathcal{L}_{OB}$ that characterizes vertical structure within the surface layer. This analysis was originally discussed in Tofsted (2000) and is based on analysis by Kaimal et al. (1972) of data collected during the 1968 Kansas experiment. Due to space considerations, the interested reader is directed to the referenced documents, since only the equations describing the spectrum and outer scale are

provided here.

The RvK spectrum can be expressed as the product of a Kolmogorov spectrum, $\Phi_K(\kappa)$, from equation 8, and a high-pass filter component,

$$\Phi_n(\kappa,\, L_o) = \Phi_K(\kappa)\, \Omega(\kappa\, L_o), \tag{11}$$

where the outer scale modulating term is expressed using a weighted sum,

$$\Omega(x) = \sum_{i=1}^{i=3} w_i\, U_1(a_i\, x), \tag{12}$$

with weighting factors, $w_i = (0.25,\, 0.50,\, 0.25)$ and frequency coefficients $a_i = (0.80,\, 2.00,\, 5.00)$, respectively, in the basic high-pass function,

$$U_1(X) = \frac{(X^2)^{17/6}}{(1+X^2)^{17/6}}. \tag{13}$$

Overall, the RvK spectrum is consistent with the spectrum of Tofsted (2007), but the above derivation clearly shows the filtering effect of $\Omega(\kappa\, L_o)$. The U_1 function also guarantees that the spectral dependence at low frequency is κ^2, consistent with von-Kármán's low frequency prescription, and with the required inertial subrange high frequency $\kappa^{-11/3}$ dependence.

The rationale for employing three shifted copies of U_1 is based on comparison between the form of U_1 and the plots of Kaimal et al. (1972). The U_1 function is narrower than reality, requiring multiple shifted copies.

At this point perhaps it would be valuable to make some comment with regard to the traditional form taken by the so-called von-Kármán (vK) spectrum. First, how this spectrum came about and who originally proposed this form is somewhat of a mystery, though it does appear in early writings of Tatarskii (1971). It is commonly expressed as,

$$\Phi_{vK}(\kappa,\, L_o) = \beta\, C_n^2\, \left[\frac{1}{(L_o^{-2}+\kappa^2)^{11/6}}\right]. \tag{14}$$

Note that this spectrum reaches a maximum at zero frequency, while von-Kármán specifically indicated a low frequency behavior of κ^2. Also, recall that the refractive index spectrum is actually the power spectrum for a space containing refractive index perturbations. That is, one subtracts from the spatially varying refractive index function its mean value. Therefore the space of refractive index perturbations has a zero mean. But the zero frequency component of the

power spectrum is just the squared mean value, which is zero. Therefore the traditionally used vK spectrum is technically incorrect while the RvK spectrum properly characterizes the behavior at the origin and reflects an energy containing range (e.g., Hinze, 1987). This is not to say that this spectrum is without faults. It assumes isotropy, which is inaccurate for larger scale perturbations, but that is a topic for a separate analysis. Perhaps a more accurate spectrum could be developed in the future that includes a flattening of the spectrum at lower frequencies, consistent with more recent analyses (e.g., Tofsted et al., 2009).

Next, we consider parameterizing the outer scale. Kaimal's results also included data that could be analyzed to form a relationship between the outer scale and height above the surface, H, and the Obukhov length, L_{OB}. In this process it also became obvious that standard spectral forms containing an outer scale simply included L_o as a parameter, but without attaching that parameter to any physically meaningful property of the atmosphere. As such, the best course appeared to argue that a specific definition of outer scale be stated: Let $\kappa_o = 1/L_o$, such that the outer scale may be defined as,

$$\Phi_n(1/L_o,\, L_o) \Big/ \Phi_K(1/L_o) = 1/2. \tag{15}$$

The outer scale is thus just the 3-dB level of the Revised von-Kármán spectrum relative to the Kolmogorov spectrum. As a matter of interest, one may also define an integral scale, Λ_o, representing the peak of the overall spectrum, which we expect to occur roughly in the center of the "Energy Containing Range" (Hinze, 1987). This scale occurs approximately at $\Lambda_o = 2\, L_o$.

Based on this outer scale definition, the Kaimal et al. plot results could be analyzed (Tofsted, 2000), and the outer scale modeled as,

$$L_o = \begin{cases} H/(4.34\sqrt{+\xi} + 0.013), & \xi > 0, \\ H/(0.34\sqrt{-\xi} + 0.013), & \xi < 0, \end{cases} \tag{16}$$

where $\xi = H/\mathcal{L}_{OB}$ is a dimensionless height ratio. Note that for large ξ argument, the outer scale increases roughly as a function of $(H\,|\mathcal{L}_{OB}|)^{1/2}$. In general $\mathcal{L}_{OB} < 0$ during daylight hours when the sensible heat flux is positive (ground is heating the air), and $\mathcal{L}_{OB} > 0$ at night when this situation is reversed. Thus L_o is generally larger during the daytime than at night, even at the same height, a result that generally conflicts with the commonly used approximation $L_o \approx k\, H$, where $k \approx 0.4$ is von-Kármán's constant.

To determine the impact of this spectrum on angle-of-arrival, we examine the influence of the spectrum on wave and phase structure functions, and the resulting influence on the angle-of-arrival variance based on the equations in section 2. In order to compare these new

results with the prior Kolmogorov-based results, the new expressions will be derived in forms consistent with Fried's original analysis.

4. Outer Scale and Diffraction Influenced Angle-of-Arrival

Using the Fried angle-of-arrival formulation described in section 2, we first describe the results of that analysis for Kolmogorov turbulence, then consider the influence of the outer scale along with diffraction effects. However, from the point of view of developing the results, we need to work backwards, starting with the wave structure function, then dealing with the phase structure function, which contains a diffraction related component, and finally the Kolmogorov based angle-of-arrival variance. We can then work this same process for the Revised von-Kármán spectrum.

Let us begin by repeating the equation for the wave structure function:

$$\mathcal{D}(\rho) = 8\,\pi^2\,k^2\,L\int_0^1 \mathrm{d}c\int_0^\infty \kappa\,\mathrm{d}\kappa\,\Phi_n(\kappa)\,\left[1 - J_0(\kappa\,c\,\rho)\right]. \tag{17}$$

To simplify the integrals, we let $V = \kappa\,c\,\rho = \kappa\,c\,Du$ replace the Bessel function argument. We then transform the argument of the spectral inner integral to one extending over V:

$$\mathcal{D}(Du) = 8\,\pi^2\,\beta\,k^2\,L\,C_n^2\,D^{+5/3}\,u^{+5/3}\int_0^1 c^{+5/3}\,\mathrm{d}c\int_0^\infty V^{-8/3}\,\left[1 - J_0(V)\right]\,\mathrm{d}V. \tag{18}$$

For constant turbulence conditions the inner and outer integrals are separable, where,

$$\int_0^1 c^{+5/3}\,\mathrm{d}c = \frac{3}{8}, \qquad \int_0^\infty V^{-8/3}\,\left[1 - J_0(V)\right]\,\mathrm{d}V = \aleph \approx 1.1183344. \tag{19}$$

These results allow us to define a nominal coherence length,

$$\widehat{\rho}_o^{-5/3} = 4 \times \frac{3}{8}\pi^2\,\beta\,\aleph\,k^2\,L\,C_n^2, \tag{20}$$

such that the wave structure function for constant Kolmogorov turbulence may be expressed, using $S = D/\widehat{\rho}_o$,

$$\mathcal{D}(Du) = 2\,\widehat{\rho}_o^{-5/3}\,u^{+5/3}\,D^{+5/3} = 2\,S^{5/3}\,u^{5/3}. \tag{21}$$

Using this form, we next consider the effect of diffraction on the phase structure function. This result was previously discussed in Tofsted (2011). As before, we repeat the phase structure

function equation:

$$\mathcal{D}_\phi(\rho) = 8\,\pi^2\,k^2\,L\int_0^1 \mathrm{d}c\int_0^\infty \kappa\,\mathrm{d}\kappa\,\Phi_n(\kappa)\,\left[1 - J_0(\kappa\,c\,\rho)\right]\,\cos^2\left[\frac{\kappa^2\,\lambda\,L\,c(1-c)}{4\pi}\right]. \qquad (22)$$

Again introducing the same dimensionless variable $V = \kappa\,c\,\rho = Duc\kappa$, and again utilizing $\widehat{\rho}_o$, the double integral form can be expressed as,

$$\mathcal{D}_\phi(Du) = 2\left(\frac{Du}{\hat{\rho}_0}\right)^{5/3}\int_0^1 \frac{c^{5/3}\,\mathrm{d}c}{(3/8)}\int_0^\infty \mathrm{d}V\,\frac{V^{-8/3}}{\aleph}\,\left[1 - J_0(V)\right]\,\cos^2\left[\frac{V^2}{(Qu)^2}\,\frac{c(1-c)}{4\pi\,c^2}\right]. \qquad (23)$$

Clearly the double integral is only a function of Qu, reflecting the influence of diffraction. Following a similar methodology as in previous papers on the topic of the phase structure function, we now write this function as,

$$\mathcal{D}_\phi(Du) = 2\,(Su)^{5/3}\,\alpha(Qu) = \mathcal{D}(Du)\,\alpha(Qu), \qquad (24)$$

where,

$$\alpha(Qu) = \int_0^1 \frac{c^{5/3}\,\mathrm{d}c}{(3/8)}\int_0^\infty \mathrm{d}V\,\frac{V^{-8/3}}{\aleph}\,\left[1 - J_0(V)\right]\,\cos^2\left[\frac{V^2}{(Qu)^2}\,\frac{c(1-c)}{4\pi\,c^2}\right]. \qquad (25)$$

The form taken by this function is plotted in figure 1 for ten decades of $R = Qu$ variation.

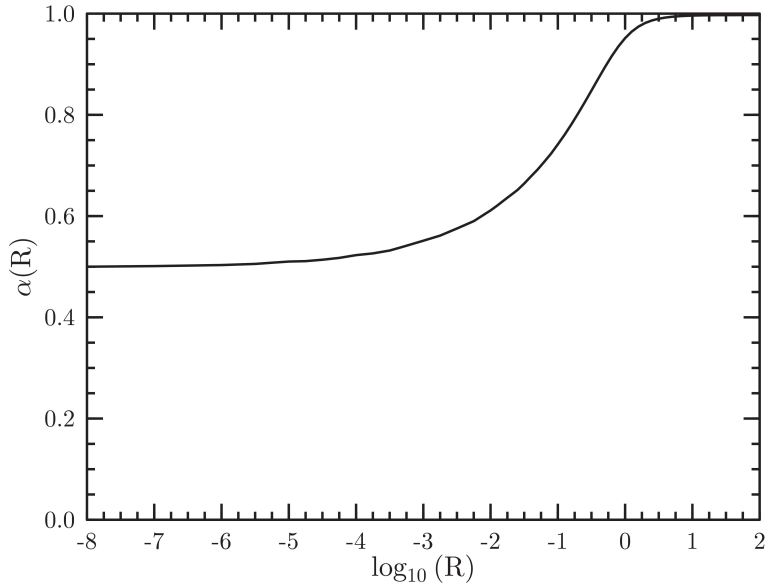

Figure 1. Phase structure function diffraction dependence factor $\alpha(R)$, with $R = Qu$, for constant Kolmogorov turbulence.

Introducing the equation 24 representation of the phase structure function into the equation 3 tilt parameter variance equation, and then introducing this result into equation 5, we produce an equation for the angle-of-arrival variance of

$$\left\langle \alpha^2 \right\rangle = \frac{128\, S^{5/3}}{k^2\, D^2} \int_0^1 du\ \left[\mathcal{F}_C(u) - \mathcal{F}_L(u)\right]\, u^{8/3}\, \alpha(Q\, u). \tag{26}$$

The integral over the system aperture is clearly a function of Q alone, which may be further normalized relative to the limiting response at $Q \to \infty$, where $\alpha = 1$. In this limit, the component integrals evaluate to,

$$\int_0^1 du\, \mathcal{F}_C(u)\, u^{8/3} \approx 0.03749; \qquad \int_0^1 du\, \mathcal{F}_L(u)\, u^{8/3} \approx 0.00489. \tag{27}$$

such that $128 \times (0.03749 - 0.00489) = 4.1728$, and the angle-of-arrival variance may be expressed as,

$$\left\langle \alpha^2 \right\rangle = 4.1728\, S^{5/3}\, G(Q)/(k^2\, D^2). \tag{28}$$

The function $G(Q)$, thus defined, is plotted in figure 2. This function assumes near–limiting behavior $G(Q) \approx 1$ for $Q > 3$.

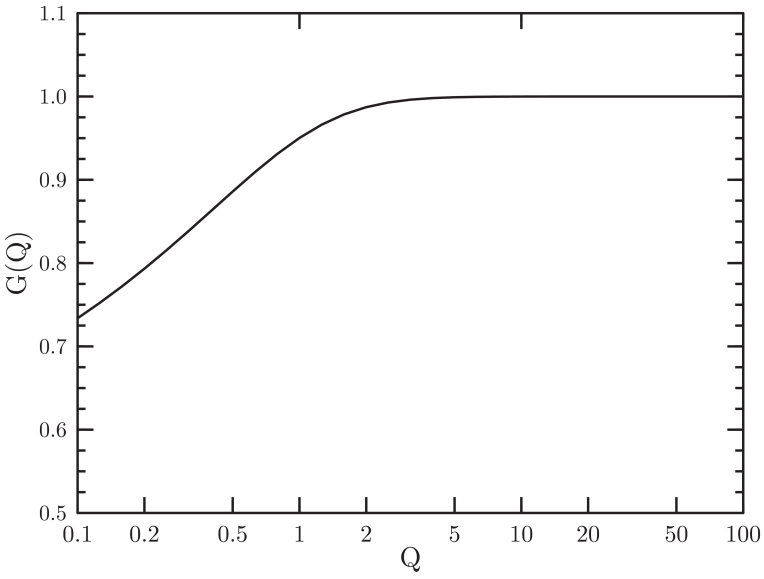

Figure 2. Angle-of-arrival variance diffraction dependence function $G(Q)$, with $Q = D/\sqrt{\lambda L} = D/P$, for constant Kolmogorov turbulence.

Comparison of this result with the Dror and Kopeika (1995) and Beland (1993) equations requires

expanding $S^{5/3} = (D/\widehat{\rho}_o)^{5/3}$ such that the limit at large Q can be expressed as,

$$\left\langle \alpha^2 \right\rangle = 4.1728\,(3/2)\,\pi^2\,\beta\,\aleph\,L\,C_n^2/D^{1/3} = 2.2798\,L\,C_n^2/D^{1/3}. \tag{29}$$

For constant C_n^2, Dror and Kopeika's equation leads to a scaling factor of $2 \times 2.92 \times (3/8) = 2.19$ corresponding to the full angle-of-arrival variance. Comparing the lead constants of Beland (equation 1) and that used by Dror and Kopeika (equation 2), apparently the Beland result corresponds to a single-axis angle-of-arrival, rather than the full angle-of-arrival variance.

In a more recent publication (Tofsted, 2012) the question of path varying turbulence strength was addressed, revealing that this variation can be accounted for through rescaling of the S and Q parameters. Thus the above forms are identical for variable path height geometries. However, the introduction of path varying outer scale might introduce unusual changes in the wave and phase structure functions. Therefore, in this initial study, only path constant outer scale influences will be considered.

Given that caveat, we are now prepared to extend the angle-of-arrival analysis to the case of the RvK turbulence spectrum. Following the pattern established when studying angle-of-arrival for Kolmogorov turbulence, we first direct our attention on the wave structure function. Introducing the outer scale influenced spectrum in equation 17, the argument to the Bessel function can again be replaced by the variable V, but the resulting double integral no longer factors as two independent integrals. Instead, a dependence on the dimensionless variable Zuc appears:

$$\mathcal{D}(Du) = 8\,\pi^2\,\beta\,k^2\,L\,C_n^2\,(Du)^{+5/3} \int_0^1 c^{+5/3}\mathrm{d}c \int_0^\infty \Omega\left(\frac{V}{Zuc}\right) \frac{[1 - J_0(V)]}{V^{8/3}}\,\mathrm{d}V. \tag{30}$$

We may, nevertheless, divide through the double integral by the factor $(3/8)\,\aleph$ such that we may again express the function in terms of the nominal coherence length $\widehat{\rho}_o$ from equation 20. The complete wave structure function may thus be expressed using a form similar to equation 21,

$$\mathcal{D}(Du) = 2\,(Su)^{5/3}\,H(Zu), \tag{31}$$

where the new outer-scale dependent function,

$$H(Zu) = \int_0^1 \frac{c^{+5/3}}{(3/8)}\mathrm{d}c \int_0^\infty \Omega\left(\frac{V}{Zuc}\right) \frac{[1 - J_0(V)]}{\aleph\,V^{8/3}}\,\mathrm{d}V, \tag{32}$$

is introduced. Now note that the Ω factor approaches unity at large argument. Thus, for small Z, the integral approaches the limiting Kolmogorov behavior. That is, $H(Zu)$ must have a limit of

unity at small Zu. Conversely, for large Z, the outer scale influence will dominate. In this limit it is advantageous to introduce yet another dimensionless constant, $M = L_o/\widehat{\rho}_o$, along with the function $H_H(x) = x^{5/3}\, H(x)$, such that,

$$\mathcal{D}(Du) = 2\, M^{5/3}\, H_H(Zu). \tag{33}$$

$H_H(Zu)$ approaches a constant limit as $Zu \to \infty$, $\mathcal{D}(\infty) \approx 8.40\, M^{5/3}$; $H_H(\infty) = 4.20$. The function $H_H(Zu)$ is plotted in figure 3, along with the small scale asymptotic dependence $(Zu)^{5/3}$.

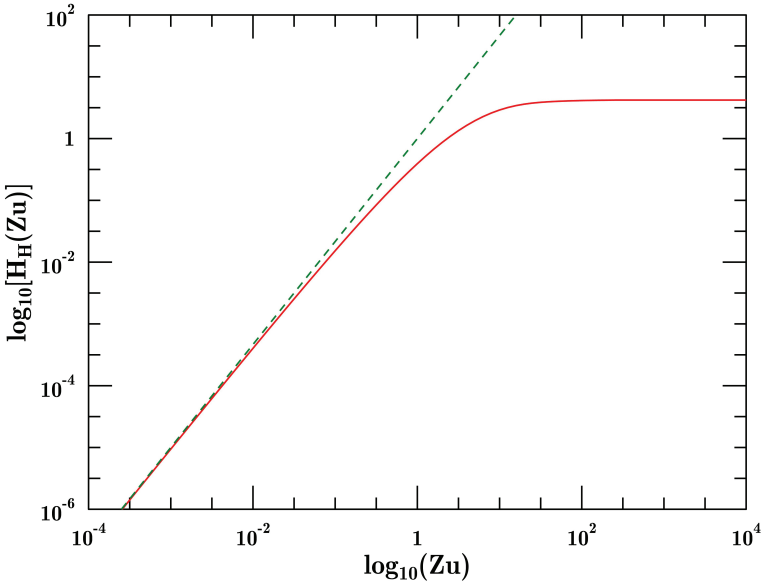

Figure 3. Outer scale cutoff of the wave structure function (solid line) compared to $(Zu)^{5/3}$ power law for Kolmogorov wave structure function.

The effect of the outer scale limitation on the refractive index spectrum is such that the wave structure function exhibits an upper limit. Equivalently, the function $H(Zu)$ must be proportional to $(Zu)^{-5/3}$ for large Zu such that $\mathcal{D}(\rho)$ approaches a finite upper bound.

Using the modified equation 33 wave structure function, we next explore the extension of the outer scale impacts to the phase structure function. To express this structure function for the RvK model, we again use the V variable, and pull the cosine-squared term from equation 25, to produce,

$$\mathcal{D}_\phi(Du) = 2\,(Su)^{5/3} \int_0^1 \frac{c^{5/3}\,\mathrm{d}c}{(3/8)} \int_0^\infty \mathrm{d}V\, \frac{[1 - J_0(V)]}{\aleph\, V^{8/3}}\, \Omega\left(\frac{V}{Zuc}\right) \cos^2\left[\frac{V^2}{(Qu)^2}\,\frac{(1-c)}{4\pi\, c}\right]. \tag{34}$$

Following the model of the analysis for Kolmogorov turbulence, the wave structure function effects are extracted, leaving a function of both Qu and Zu, reflecting the influences of both diffraction and outer scale. The phase structure function may thus be expressed as,

$$\mathcal{D}_\phi(Du) = \mathcal{D}(Du)\, A(Qu,\, Zu) = 2\,(Su)^{5/3}\, H(Zu)\, A(Qu,\, Zu), \tag{35}$$

where,

$$A(Qu,\, Zu) = \int_0^1 \frac{c^{5/3}\,\mathrm{d}c}{(3/8)} \int_0^\infty \mathrm{d}V\, \frac{[1 - J_0(V)]}{\aleph\, V^{8/3}}\, \frac{\Omega[V/(Zuc)]}{H(Zu)}\, \cos^2\!\left[\frac{V^2}{(Qu)^2}\, \frac{(1-c)}{4\pi\, c}\right]. \tag{36}$$

The form taken by this two-dimensional function is plotted for a series of values of Qu as functions of Zu in figure 4. Zu varies over the range from 10^{-8} to 10^{+4}, exhibiting near-asymptotic behaviors at both extremes. The Qu values ranged from $Qu = 2^{-6}$, for the lowest curve, to 2^{+6} for the highest curve, in increments of factors of 2 between consecutive curves.

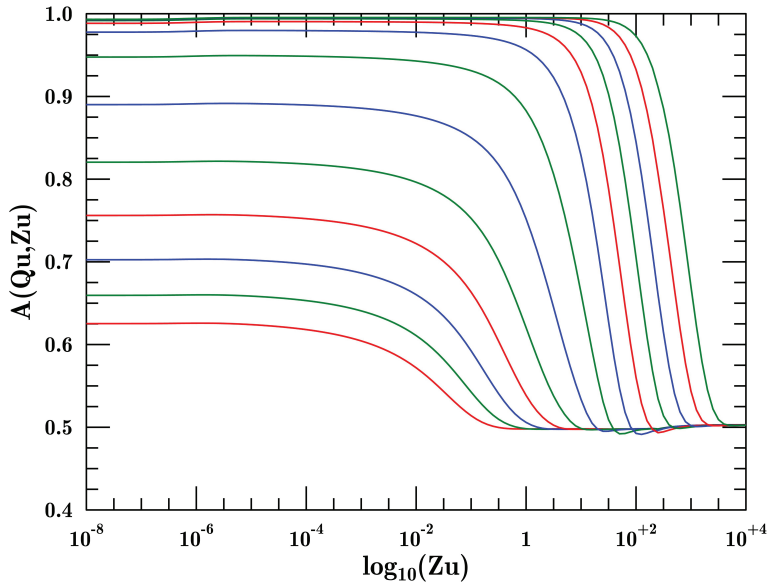

Figure 4. Outer scale impact on transition function of phase structure function. 13 plots of different Qu values from 2^{-6} (bottom-most curve) to 2^{+6} (upper-most curve) differing by a factor of 2 between each.

To compare the behavior of $A(Qu, Zu)$ with that of $\alpha(Qu)$, we consider the limit $Zu \ll 1$. To compare these cases we plot the $A(Qu, 10^{-8})$ against $\alpha(Qu)$ in figure 5. As expected, the asymptotic behavior of $A(Qu, Zu)$ ranges between 0.5 and 1.0 at $Zu \ll 1$, corresponding to the

asymptotic behaviors of $Qu \ll 1$ and $Qu \gg 1$, respectively, seen in figure 1. The range of Qu selected is characteristic of most imaging scenarios except for extremely large or small optics.

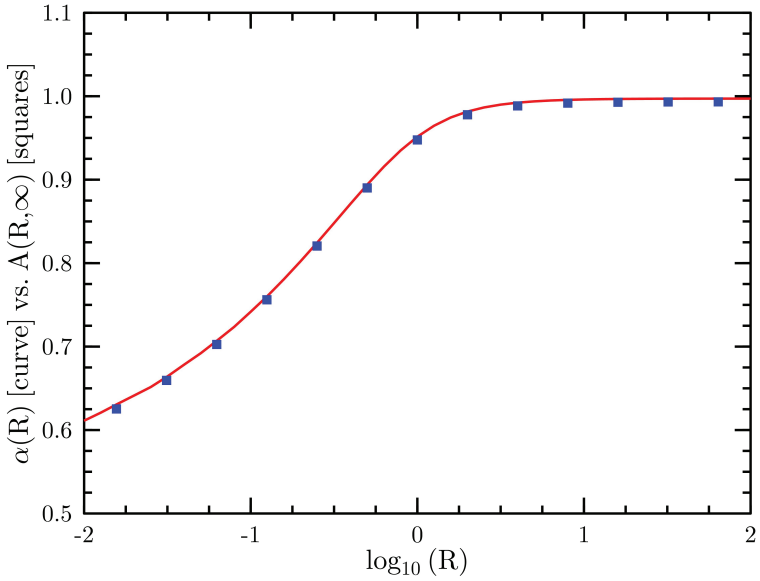

Figure 5. Comparison of $\alpha(R)$ from the Kolmogorov turbulence model, versus $A(R, Zu)$ from the Revised von Kármán turbulence model, with $R = Qu$.

For the remaining behavior of $A(Qu, Zu)$, obviously the function exhibits a complicated behavior that defies easy characterization. So, rather than attempting to characterize this intermediate result, let us instead continue on to determine the angle-of-arrival variance for RvK turbulence.

Introducing the tabulated $A(Qu, Zu)$ results into a numerical integration routine, we begin with equation 26 as modified by the RvK phase structure function:

$$\langle \alpha^2 \rangle = \frac{128\, S^{5/3}}{k^2\, D^2} \int_0^1 \mathrm{d}u\ [\mathcal{F}_C(u) - \mathcal{F}_L(u)]\ u^{8/3}\, H(Zu)\, A(Qu,\, Zu). \tag{37}$$

Now, the results of this integration will approach those of the equation 27 limiting behaviors when $Zu \ll 1 \ll Qu$. Therefore, for comparison purposes we may multiply and divide by the factor 0.03260 = 0.03749 - 0.00489. This produces the same lead coefficient as in equation 29 such that we can write,

$$\langle \alpha^2 \rangle = 2.2798\, L\, C_n^2 / D^{1/3}\, G_G(Q, Z), \tag{38}$$

where,

$$G_G(Q, Z) = \int_0^1 \mathrm{d}u\, \frac{[\mathcal{F}_C(u) - \mathcal{F}_L(u)]}{0.03260}\, u^{8/3}\, H(Zu)\, A(Qu, Zu). \tag{39}$$

Like the $G(Q)$ function, the $G_G(Q, Z)$ function will approach unity when $Z \ll 1 \ll Q$, but will then decay when this condition does not hold. This function is plotted for a range of Q values as a function of Z in figure 6.

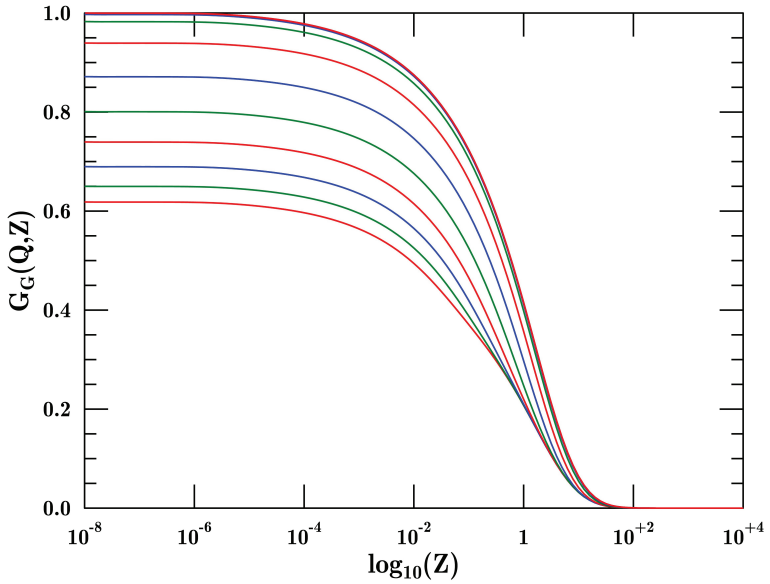

Figure 6. Weighting function $G_G(Q, Z)$ for the range $10^{-8} < Z < 10^{+4}$ and $2^{-6} < Q < 2^{+6}$ (lowest to highest curves).

Figure 7 then shows the similarity in the limiting behavior of $G_G(Q, Z)$ at low values of Z compared to the behavior of $G(Q)$ from figure 2. From this comparison we observe an apparent correlation between the effects of small Z and small Q in the $G_G(Q, Z)$ model such that at low Q G_G tracks increasingly below $G(Q)$ as Q drops.

5. Discussion

We thus have developed a picture of the behavior of the angle-of-arrival variance as the outer scale and diffraction effects vary. However, as we also have a means of connecting the atmospheric propagation characteristics to typical meteorological characteristics, let us consider what we might encounter as typical effects. To begin, let us select a typical windspeed of 3.5 m/s. This is characteristic of a daytime desert atmosphere (c.f., figure 14 of Tofsted et al. (2009), where we considered mean hourly windspeeds collected over a 60 day period in 2008). Let us also consider a path height of $H = 4$ m AGL (above ground level). Typical daytime

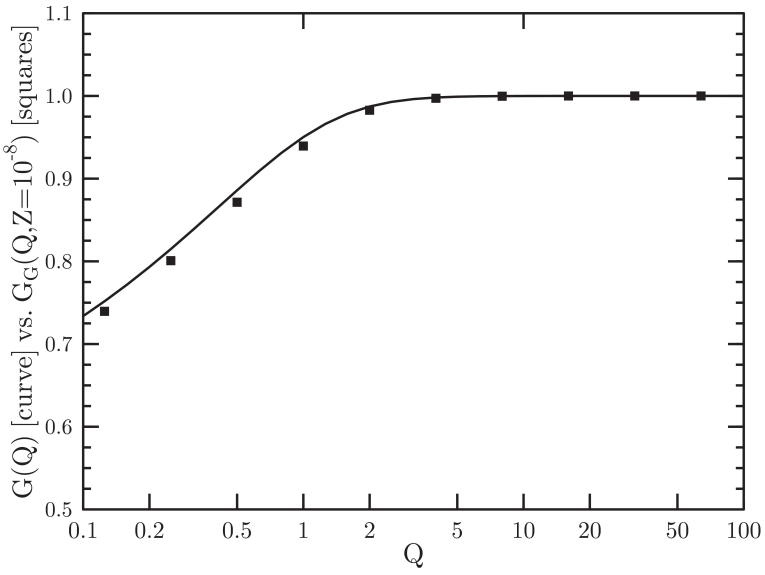

Figure 7. Comparison of $G(Q)$ function plotted in figure 2 against the $G_G(Q, Z)$ from figure 6 for small Z.

temperatures during our measurement period averaged around 25 °C or roughly 300 K. The White Sands area stands at approximately 1400 m ASL (above sea level) with typical atmospheric pressure of $P = 880$ mbar (millibars), and characteristic sensible heat flux values were in the range 200–600 W/m^2. We write the equation for the Obukhov length as (Tofsted, 1993),

$$L_{Ob} = -\frac{\rho\, C_P\, T\, u_\star^3}{k\, g\, \mathcal{H}_S}, \tag{40}$$

where ρ is the dry air density,

$$\rho = 0.34838\, P/T, \tag{41}$$

with pressure P in millibars, and temperature T in Kelvin, such that ρ is expressed as kg/m^3; C_P is the heat capacity of air at constant pressure, 1004.84 J/(kg K); k is von-Karman's constant, $k \approx 0.4$; g is the gravitational attraction, $g = 9.81$ m/s^2; $u_\star$ is the friction velocity in m/s; and $\mathcal{H}_S$ is the sensible heat flux. While the true friction velocity exhibits an effect due to *diabatic* influences, for the sake of simplicity here we use only the logarithmic wind profile, such that ψ_m, the momentum diabatic function, is zero, and we posit,

$$u_* = \frac{k\, u}{\ln(H/H_o) - \psi_m} \approx \frac{k\, u}{\ln(H/H_o)}, \tag{42}$$

where H_o is the surface roughness length (Hansen, 1980), which we determined through

measurements to be approximate 4.5 cm, which approximately matches Hansen's recommended relative length compared to typical roughness element heights of 1 m (mesquite bushes, grass, and yuccas plants). For a 2-m-wind measurement height, and wind speed $u = 3.5$ m/s, we thus estimate a friction velocity of $u_* \approx 0.37$ m/s.

The atmospheric density is approximately $\rho = 1.022$ kg/m^3. Hence, $\rho C_P = 1026.9$ J/(m^3 K), such that $\mathcal{Q} = \mathcal{H}_S/(\rho C_P)$ will range from 0.195 to 0.584 K m/s. Therefore, we can express the range of the Obukhov length as,

$$L_{Ob} = -\frac{T u_\star^3}{k g \mathcal{Q}} = -20 \text{ m} ... -7 \text{ m}. \tag{43}$$

For this range of Obukhov length we obtain from equation 16 a range of outer scale from 14 m to 24 m for a path height of 4 m, where the outer scale is shorter under stronger turbulence conditions.

Consider then a range of optics aperture sizes ranging from 2.5 cm for binocular optics to 20 cm for a telescope optic. For this range of the parameter D, let us also consider path length ranging from 1 km to 4 km and wavelength equal to 0.55 μm (visible radiation), or a range of $P = (\lambda L)^{1/2}$ of 2.35 cm to 4.7 cm.

For $D = 2.5$ cm, $Z = D/L_o$ ranges from 0.0010 to 0.0018, while $Q = D/P$ varies from 0.53 to 1.06. Hence, from figure 6 the G_G coefficient varies from 0.85 to 0.90 where the impacts of Q and Z are approximately equal.

For $D = 20$ cm, Z ranges from 0.0083 to 0.0143, while Q varies from 4.26 to 8.51, and G_G varies from 0.88 to 0.93 where the impact is virtually all due to variations in Z.

Overall, the scaling constant from figure 6 is between 0.80 and 0.95, or (in combination with the scaling constant 2.28 from equation 38) when compared to the constant 2.19 derived from equation 2, one obtains a range from 1.824 to 2.17. That is, angle-of-arrival variance ratios range from 0.833 to 0.989. Of course, if we intend to use angle-of-arrival variance to compute C_n^2, we recognize that turbulence strength is highly variable, often exhibiting a third of an order of magnitude variance around a mean with correlation times on the order of several seconds or less. Also, since most imaging scenarios involve Q values greater than unity, and usually of the order 2 or greater, we expect that the outer scale influence (rather than diffraction) will be the dominant term, and this impact does extend down to produce a 10% effect even for Z values on the order of 0.01, and not, as Dror and Kopeika indicated, merely $Z < 1$.

6. Conclusions

In this study a new analysis of the influence of both diffraction and outer scale of turbulence effects on angle-of-arrival variance has been performed. This analysis has shown that outer scale influences can be significant even for aperture sizes far less than the outer scale size. To use the information developed in this report, one can simply apply rule-of-thumb estimates in determining the Obukhov length, plus estimates of the optical path height, to determine the outer scale. From this knowledge, and knowledge of the system aperture size, one can easily determine the correction necessary to obtain a more accurate estimate of C_n^2 from observed edge motion analysis.

This analysis has also shown the relative strengths and weaknesses in previous analyses. In particular, the Dror and Kopeika (1995) equation appears to be roughly correct as long as $Z \ll 1 < Q$. However, this condition differs from that indicated by Dror and Kopeika of $Z < 1 \ll Q$. More generally, the new formulation provides a method of estimation under a far wider set of measurement conditions than that supported by previous analyses. Also, Tofsted (1992) only considered the outer edge of the wave propagating toward the aperture when evaluating angle-of-arrival variance. The current analysis is obviously more suitable for circular aperture systems involving an ensemble of point separations in the aperture.

7. References

Beland, R. R. Propagation through Atmospheric Optical Turbulence, Chapter 2 of *Atmospheric Propagation of Radiation*, Vol. 2 of the Infrared & Electro-Optical Systems Handbook, F. G. Smith, ed., pp. 157–232, (SPIE Optical Engineering Press, Bellingham, WA, 1993).

Dror, I.; Kopeika, N. S. Experimental Comparison of Turbulence Modulation Transfer Function and Aerosol Modulation Transfer Tunction Through the Open Atmosphere. *J. Opt. Soc. Am. A* **1995** *12*, 970–980.

Fried, D. L. Optical Resolution Through a Randomly Inhomogeneous Medium for Very Long and Very Short Exposures. *J. Opt. Soc. Am.***1966** *56*,1372–1379.

Goodman, J. W. *Statistical Optics*; J. Wiley & Sons, 1985.

Hansen, F. V. *The Extrapolation of the Wind Profile with Height*, ASL Internal Report, U.S. Army Atmospheric Sciences Laboratory: White Sands Missile Range, NM 88002-5501 (1980).

Hinze, J. O. *Turbulence*; MacGraw Hill, New York, NY, 1987.

J. C. Kaimal, J. C. Wyngaard, Y. Izumi, and O. R. Coté, "Spectral characteristics of surface-layer turbulence," *Q. J. Roy. Met. Soc.*, **98**:563-589 (1972).

Obukhov, A. M. Turbulence in an Atmosphere with a Non-Uniform Temperature, *Trudy In-ta Teoret Geofiz, AN SSSR, (Works Inst Theor Geophys Acad Sci, USSR)* **1946**, *1*, 95–115 (English translation in *Boundary Layer Meteorology* **1971**, *2*, 7–29).

Paulson, C. A. The Mathematical Representation of Wind Speed and Temperature Profiles in the Unstable Atmospheric Surface Layer. *J. Appl. Meteorol.* **1970**, **9**, 857–861.

Tatarskii, V. I. *The Effects of the Turbulent Atmosphere on Wave Propagation*, translation for NOAA by Israel Program for Scientific Translations, Jerusalem (1971).

Tofsted, D. H. Short-Exposure Passive Imaging Through Path-Varying Convective Boundary Layer Turbulence. *Proc. SPIE* **2012**, *8355*, 83550J-1-12.

Tofsted, D. H. Reanalysis of turbulence effects on short–exposure passive imaging. *Opt. Eng.* **2011**, *50*, 016001.

Tofsted, D. H.; O'Brien, S.; Klipp, C.; Yarbrough, J.; Quintis, D.; Brice, R.; Bustillos, M.; Elliott, S.; Creegan, E. *Three-Dimensional Turbulence Measurements in the Atmospheric Surface Layer: Experimental Design and Initial Analysis*; ARL-TR-4953; U.S. Army Research Laboratory: White Sands Missile Range, NM 88002-5501, 2009.

Tofsted, D. H.; O'Brien, S.; Yarbrough, J.; Quintis, D.; Bustillos, M. "Characterization of Atmospheric Turbulence During the NATO RTG-40 Land Field Trials. *Proc. SPIE* **2007**, *6551*, 65510J.

Tofsted, D. H.; O'Brien, S. G.; Vaucher, G. T. *An Atmospheric Turbulence Profile Model for Use in Army Wargaming Applications I*; ARL-TR-3748; U.S. Army Research Laboratory: White Sands Missile Range, NM 88002-5501, 2006.

Tofsted, D. H. *Turbulence Simulation: Outer Scale Effects on the Refractive Index Spectrum*; ARL-TR-548; U.S. Army Research Laboratory: White Sands Missile Range, NM 88002-5501, 2000.

Tofsted, D. H. *A Surface Energy Budget Model Modifying Heat Flow by Foliage Effects*; ARL-TR-60; U.S. Army Research Laboratory: White Sands Missile Range, NM 88002-5501, 1993.

Tofsted, D. H. Outer-scale Effects on Beam-wander and Angle-of-Arrival Variances. *Appl. Opt.* **1992**, *31*, 5865–5870.

von Kármán, T. Progress in the Statistical Theory of Turbulence. *Proc. Natl. Acad. Sci. U.S.* **1948**, *34*, 530–539.

NO. OF COPIES	ORGANIZATION
1 ELEC	ADMNSTR DEFNS TECHL INFO CTR ATTN DTIC OCP 8725 JOHN J KINGMAN RD STE 0944 FT BELVOIR VA 22060-6218
1 CD	US ARMY NIGHT VISION & ELECTRONICS SENSORS DIRECTORATE SENSOR PERFORMANCE BRANCH ATTN AMSRD CER NV MS SP R ESPINOLA 10221 BURBECK RD FT BELVOIR VA 22060-5806
1 CD	STARFIRE OPTICAL RANGE ATTN AFRL RDS T FARRELL KIRTLAND AFB ALBUQUERQUE NM 87117
1 CD	DRDC VALCARTIER ATTN G POTVIN 3701 CARLING AVE OTTAWA ONTARIO K1A 0Z4 CANADA
1 CD	US ARMY RSRCH LAB ATTN RDRL CIE D R BRICE WHITE SANDS MISSILE RANGE NM 88002
1 CD	US ARMY RSRCH LAB ATTN RDRL CIE M R SHIRKEY BLDG 1622 WHITE SANDS MISSILE RANGE NM 88002
1 CD	US ARMY RSRCH LAB ATTN RDRL CIE D D HOOCK BATTLEFIELD ENVIR DIV BLDG 1622 WHITE SANDS MISSILE RANGE NM 88002-5001
2 CDS	US ARMY RSRCH LAB ATTN RDRL CIE D D TOFSTED WHITE SANDS MISSILE RANGE NM 88002-5501
2 CDS	US ARMY RSRCH LAB ATTN RDRL CIE D M S DARCY ATTN RDRL CIE D S OBRIEN WHITE SANDS MISSILE RANGE NM 88002-5501
1 CD	US ARMY RSRCH LABORATORY ATTN RDRL CIE D E CREEGAN BLDG 1622, ROOM 201 WHITE SANDS MISSILE RANGE NM 88002
4 CDS	US ARMY RSRCH LAB ATTN IMAL HRA MAIL & RECORDS MGMT ATTN RDRL CIE D C KLIPP ATTN RDRL CIO LL TECHL LIB ATTN RDRL CIO LT TECHL PUB ADELPHI MD 20783-1197

TOTAL: 16 (1 PDF, 15 CDS)